JACS
JOURNAL OF THE AMERICAN CHEMICAL SOCIETY

ARTICLE

pubs.acs.org/JACS

Tunneling Currents That Increase with Molecular Elongation

Ignacio Franco,*[,†] Gemma C. Solomon,[‡] George C. Schatz,[†] and Mark A. Ratner*[,†]

[†]Department of Chemistry, Northwestern University, Evanston, Illinois 60208-3113, United States

[‡]Nano-Science Center and Department of Chemistry, University of Copenhagen, Universitetsparken 5, 2100 Copenhagen Ø, Denmark

Supporting Information

ABSTRACT: We present a model molecular system with an unintuitive transport−extension behavior in which the tunneling current increases with forced molecular elongation. The molecule consists of two complementary aromatic units (1,4-anthracenedione and 1,4-anthracenediol) hinged via two ether chains and attached to gold electrodes through thiol-terminated alkenes. The transport properties of the molecule as it is mechanically elongated in a single-molecule pulling setting are computationally investigated using a combination of equilibrium molecular dynamics simulations of the pulling with gDFTB computations of the transport properties in the Landauer limit. Contrary to the usual exponential decay of tunneling currents with increasing molecular length, the simulations indicate that upon elongation electronic transport along the molecule increases 10-fold. The structural origin of this inverted trend in the transport is elucidated via a local current analysis that reveals the dual role played by H-bonds in both stabilizing π-stacking for selected extensions and introducing additional electronic couplings between the complementary aromatic rings that also enhance tunneling currents across the molecule. The simulations illustrate an inverted electromechanical single-molecule switch that is based on a novel class of transport−extension behavior that can be achieved via mechanical manipulation and highlight the remarkable sensitivity of conductance measurements to the molecular conformation.

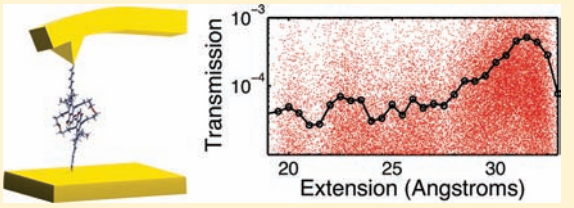

INTRODUCTION

Understanding charge transport behavior of a molecule bridging two metallic electrodes is of importance for the goal of creating nanoscale electronic devices and also offers fundamental insights into electron transfer events in donor−acceptor chemical and biological systems.[1−7] One basic physical property that is often considered is the dependence of the charge transfer rate on the molecular length ξ.[8−16] Known examples of this dependence show a characteristic decay in the rate with increased ξ in both the tunneling and activated hopping regimes. In the tunneling case, the usual exponential decay of the current $I \propto \exp[-\beta\xi]$ with increased molecular extension (where $\beta > 0$ is the decay parameter) stems from the exponential dependence of the nonresonant tunneling probability on the barrier width.[17] The hopping mechanism, in turn, observes a weaker decay of the current with molecular length[14] as $I \propto 1/(\alpha_1 + \alpha_2 N)$, where N, the number of hopping sites, is a measure of the molecular length and α_i are characteristic constants of the molecule and its coupling with the thermal environment.

Experimentally, the usual way to study the dependence of the transport properties on the molecular length is by considering a homologous series of molecules and determining how the transport characteristics change as one progresses across the series.[8−13,18] Examples of measured β parameters obtained in this fashion include 0.2−0.3 Å^{-1} for conjugated polymers,[10−12,19] 0.8−1 Å^{-1} for alkanes,[20−23] and ∼0.6 Å^{-1} for a π-stacked system.[13] Alternatively, it is also possible to study such a dependency via mechanical control of the molecular length by pulling a molecule bound to a metallic surface using a conducting atomic force microscope (CAFM) tip. Scheme 1 shows the general setup of this class of experiments. In them, the distance between the surface and the cantilever L is controlled while the molecular extension ξ fluctuates. The force exerted during pulling is determined by measuring the deflection of the cantilever from its equilibrium position $F = -k(\xi - L)$, where k is the cantilever stiffness. The pulling is performed by increasing L in some prescribed fashion. Simultaneously, a voltage is applied across the junction and the resulting current measured. In this case too experimentally[24−27] and theoretically[28−30] studied examples exhibit an increase in the wire's resistance with molecular elongation.

In this paper we present a model molecular system with an unintuitive transport−extension behavior in which the tunneling current increases with molecular elongation. We propose a specific molecular system; however, we do not suggest that these results would be unique to this system. The underlying principle guiding the molecular design is that the relaxed conformation of a molecule may not maximize the interactions responsible for transport through the system and stress-induced conformational change may lead to more favorable electronic interactions and increased transport. As the conducting medium we propose the cyclophane shown in Scheme 1A in the integrated molecular electronics/force spectroscopy setup shown in Scheme 1B. The molecule consists of two complementary aromatic units, 1,4-anthracenedione and 1,4-anthracenediol, hinged via two ether chains and attached to gold electrodes through thiol-terminated

Received: June 24, 2011
Published: August 19, 2011

Scheme 1. (A) Proposed Conducting Molecule and (B) Schematic of a Single-Molecule Pulling/Molecular Electronics Setup[a]

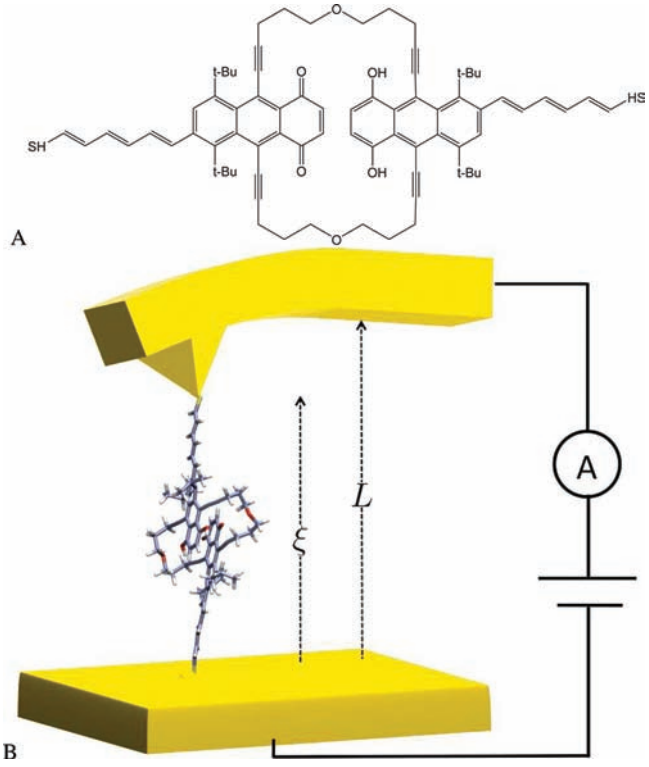

[a] The molecule is attached to a metallic surface and a conducting AFM tip through thiol−Au bonds. The distance between the surface and the cantilever (L) is controlled, a voltage is applied across the junction, and the resulting current is determined. The instantaneous applied force is given by $F(t) = -k[\xi(t) - L]$, where k is the cantilever stiffness and $\xi(t)$ is the fluctuating molecular end-to-end distance.

alkenes. The combined force-extension and molecular junction transport behavior of the molecule is theoretically characterized by combining constant temperature molecular dynamics (MD) simulations of the pulling with computations of the transport properties in the Landauer limit.[1] As shown below, the simulations indicate that the average resistance generated by this molecule decreases with elongation by mechanically opening alternative and more effective channels for the transport that are only accessible when the molecule is under strain.

Characterizing the transport behavior of single molecules under strain is a subject of considerable current interest. Collectively, correlations between molecular transport and elasticity characteristics have the potential to provide highly discriminating information about the behavior of single molecules in junctions. In addition, the AFM tip offers remarkable mechanical control over the molecular conformation, thus opening unique opportunities for the design of novel mechanically activated molecular devices. Experimental efforts to characterize extension−transport behavior in junctions include measurements of the conductance of a conjugated polymer as a continuous function of its length,[24] studies of the effect of the contact geometry on the transmission,[25,31] a demonstration of mechanically induced magnetic anisotropy in a coordination complex,[32] and a proposal to use transport−extension behavior as an analytical probe for DNA base pairs,[27] among others.[26,33] In a previous computational study,[30] we proposed a mechanically activated molecular switch that is based on unfolding a molecular π-stacker. We also identified correlated force−conductance blinking in a region of dynamical bistability as a characteristic feature of mechanoelectric nanojunctions. Related computational studies[28,29] have focused on the extension−transport behavior of alkane systems.

COMPUTATIONAL METHODOLOGY

The pulling−transport behavior of the cyclophane was characterized by combining MD simulations of the pulling[34] with electronic structure computations of the transport properties. To bridge the several orders of magnitude gap between experimentally employed pulling speeds (10^{-6}−10^{-9} m s^{-1}) and those that can be accessed computationally, the pulling was performed under reversible conditions so that the results become independent of the pulling speed. The molecule was described using the MM3 force field[35−37] and the dynamics followed using TINKER 4.2.[38] The MM3 force field adequately describes π-stacking interactions[39] and includes directional hydrogen-bonding terms important in the description of the cyclophane. Additional force field parameters required to describe the cyclophane are included in the Supporting Information.

During pulling, one terminal S atom of the molecule was attached to a rigid isotropic harmonic potential that mimics the molecular attachment to the surface. Simultaneously, the opposite terminal S was connected to a dummy atom via a virtual harmonic spring. The position of the dummy atom is the simulation analogue of the cantilever position L (Scheme 1). The varying deflection of the virtual harmonic spring measures the force exerted during the pulling. The pulling and subsequent retraction were performed by varying the distance between the surface and the cantilever from 20 to 35 Å and then back to 20 Å at a constant speed. The cantilever was taken to have a stiffness of k = 1.1 N/m along the pulling direction and to be rigid in the plane perpendicular to it. The pulling direction was defined by the vector connecting the two terminal S atoms of the complex. The dynamics of the system was propagated using a modified Beeman algorithm with a 1 fs integration time step dumping geometries every 100 ps. The system was coupled to a heat bath at 300 K using a Nosé−Hoover chain as the thermostat. The pulling speed required to recover reversible behavior was $v = 5 \times 10^{-6}$ Å/ps. We found that under such conditions the dissipative work in the pulling/retraction cycle is negligible. The total MD simulation time was 6 μs.

Electron transport was assumed to occur in the coherent tunneling regime in which the bias-dependent current $I(V)$ can be calculated from the Landauer formula[1]

$$I(V) = \frac{2e}{h}\int_{-\infty}^{\infty} \mathrm{d}E[f_{\mathrm{L}}(E,V) - f_{\mathrm{R}}(E,V)]\ T(E,V) \qquad (1)$$

Here e is the electron charge, h is Planck's constant, $f_{\mathrm{L,R}}$ are the Fermi functions of the left (L) and right (R) electrodes and T is the electronic transmission. The transmission and the Fermi function depend on the applied bias voltage V and the injection energy E of the electrons. We assume low biases for which $I \approx GV$, where $G = G_0 T(E_{\mathrm{F}})$ is the zero-bias conductance, $G_0 = 2e^2/h$ is the quantum of conductance, and $T(E_{\mathrm{F}})$ is the transmission at the Fermi energy of the electrodes. The quantity $T(E_{\mathrm{F}})$ was calculated for the 60 000 conformations dumped during the MD simulation using the gDFTB[40−44] tight-binding method. Such an efficient method is needed since proper statistical sampling requires taking into account 10^4−10^5 conformations. The electrodes were modeled by three 9 × 9 Au(111) layers with sulfur atoms chemisorbed to face-centered cubic (fcc) hollow sites, and periodic boundary conditions were used in the two directions perpendicular to the transport. Gold−sulfur distances were held constant at 1.84 Å for all calculations and were chosen according to the literature.[45] The method employed here is designed to carefully characterize fluctuations in the transmission

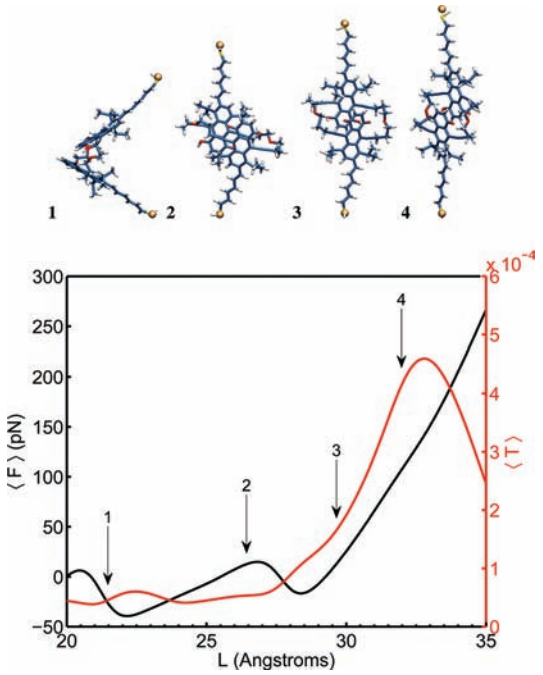

Figure 1. Average force and transmission during the extension using a cantilever of stiffness k = 1.1 N/m. Snapshots of structures encountered during pulling are included in the top panel (labels **1**−**4**). Note the increase in the average transmission as the pulling proceeds.

that are due to thermal conformational motion of the molecule. Additional conductance fluctuations that may arise due to changes of the binding site and binding distance,[46] lead-molecule interactions, and possible charging effects are not explicitly taken into account.

RESULTS AND DISCUSSION

Structural Design and Mechanical Properties. Consider first the structural design of the cyclophane studied here (Scheme 1A). The molecule consists of two complementary aromatic units joined together by two ether chains. The ethers are sufficiently flexible to allow for substantial conformational freedom of the aromatic units. The triple bond moiety that connects the ether linker to the aromatic rings is used for reducing steric hindrance between the linker and the rings. The rings have bulky *t*-Bu substituents on one side that prevent π-stacking for short extensions. For longer extensions, the *t*-Bu units no longer play a role and stacking between the aromatic rings is promoted by hydrogen-bonding interactions between the carbonyl and hydroxy functional groups in the complementary aromatic rings.

Figure 1 shows the average applied force and the average transmission across the junction during the pulling. Representative snapshots encountered during the extension (labels **1**−**4**) are shown in the upper panel. The force−extension profile during pulling (black line) indicates that there are two conformational transitions that occur as the elongation proceeds. These conformational transitions are revealed by regions of mechanical instability in the F−L isotherm where $\partial\langle F\rangle/\partial L < 0$.[34] In the first transition around $L \approx 21$ Å the planes of the aromatic rings rotate with respect to one another going from a conformation in which the *t*-Bu groups are on the same side to a conformation where they are on opposite sides. In the process the molecule adopts

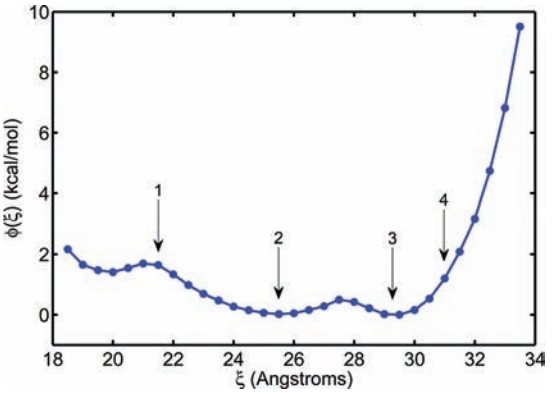

Figure 2. Molecular potential of mean force $\phi(x)$ along the end-to-end distance ξ. The numerical labels correspond to the snapshots in Figure 1.

conformations in which the two complementary aromatic rings are approximately perpendicular, **1** being an example. In the mechanically stable region between L = 22 Å and L = 27 Å the two aromatic rings are approximately parallel but not stacked. The bulky *t*-Bu groups prevent π-stacking, favoring a staggered conformation such as the one shown in **2** instead. The second conformational transition occurs around $L \approx 27.5$ Å. Around this extension the cyclophane goes from the staggered conformation to a structure where the *t*-Bu groups no longer play a dominant role and hydrogen bonding is formed between the complementary hydroxy and carbonyl groups in the aromatic units, in this way promoting π-stacking between the outermost rings in the aromatic components. Further pulling mechanically deforms this latter structure.

Naturally, these three mechanically stable regions and two conformational transitions observed in the F−L isotherms are manifest in the molecular potential of mean force (PMF) along the end-to-end distance coordinate ξ.[34] The PMF is the Helmholtz free energy profile of the molecule for fixed ξ and summarizes thermodynamic changes undergone by the molecule during pulling. Figure 2 shows the PMF reconstructed from the force−extension data using the weighted histogram analysis method (WHAM),[47,48] as described in detail elsewhere.[34] Regions of convexity along the PMF indicate mechanically stable conformations, while regions of concavity signal conformational transitions. The PMF of the cyclophane consists of three mechanically stable convex regions and two concave regions. These two regions of concavity lead to the regions of mechanical instability in the force−extension isotherm where the applied force drops with increasing extension. Representative structures characterizing the two main minima in the free energy profile are shown by **2** and **3** in Figure 1.

Molecular Conductance during Pulling. Significant electron transport across π-stacks requires favorable overlap between the aromatic rings.[49−51] Because of the structural design of the cyclophane in which the *t*-Bu prevents π-stacking for short extensions and H-bonds promote π-stacking for long extensions, the required overlap only occurs when the cyclophane is subjected to considerable strain. These structural features lead to a counterintuitive extension−transport behavior in which the transmission increases with elongation. The red line in Figure 1 shows the average transmission as a function of L. The transmission exhibits a flat profile for L = 22−27 Å where $\langle T\rangle \approx 5 \times 10^{-5}$. However, when the pulling induces a structural transition from

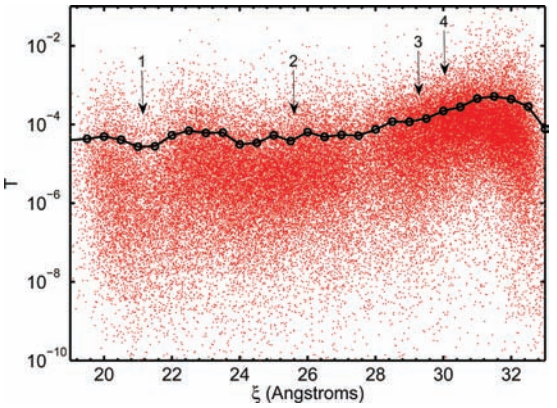

Figure 3. Transmission versus molecular end-to-end distance. Each dot corresponds to a different conformation encountered during the elongation. The black line depicts the average behavior. Note the substantial fluctuations in the transmission.

the staggered conformation **2** to the hydrogen-bonded conformation **3**, the average transmission across the junction increases by a factor of 10, peaking at 4.6×10^{-4} for $L = 32.8$ Å. Further deformation of the structure leads to a decrease in the conductance. Note that an average force of 142 pN is required to mechanically promote the configuration of maximum transmission, indicating that this highly conducting state of the cyclophane is improbable in unbiased junctions.

The transmission as a function of the molecular end-to-end distance is shown in Figure 3. In the plot, each point depicts the transmission of a conformation encountered during pulling while the black line corresponds to the average behavior. The average conductance exhibits a maximum of $(5.2 \times 10^{-4})G_0$ at $\xi = 31.5$ Å. In addition, the plot evidences the large-scale fluctuations in the transmission observed in the room temperature simulations. Transport properties of single molecules are remarkably sensitive to small conformational changes, and hence, structural variability due to thermal motion leads to fluctuations in the transmission over several orders of magnitude. From a simulation point of view the plot highlights the need to consider all thermally accessible conformations to model properly the $I-V$ characteristics of metal−molecule−metal junctions. Single conformations are simply not sufficient to characterize transport adequately in this case. Similar observations have been made in studies of the role of fluctuations in biological electron transfer.[52−54] In both cases, the important structures for predicting the transfer/transport properties are not necessarily the minimum energy structures but those structures within the thermally accessible ensemble with enhanced transfer/transport-determining electronic coupling.

To elucidate the transport mechanism during pulling, we employ the local current analysis described in detail in ref 55. In it, the total transmission is decomposed into local transmission[44,55,56] elements T_{AB} between pairs of atoms (A and B) such that the sum of local transmission elements across a surface perpendicular to the transport direction equals the total transmission:[55]

$$T(E,V) = \sum_{A \in L, B \in R} T_{AB}(E,V) \qquad (2)$$

where A and B are atoms located to the left (L) or right (R) of the surface in question. The derivation of eq 2 and the explicit expression for $T_{AB}(E,V)$ have been presented before.[55]

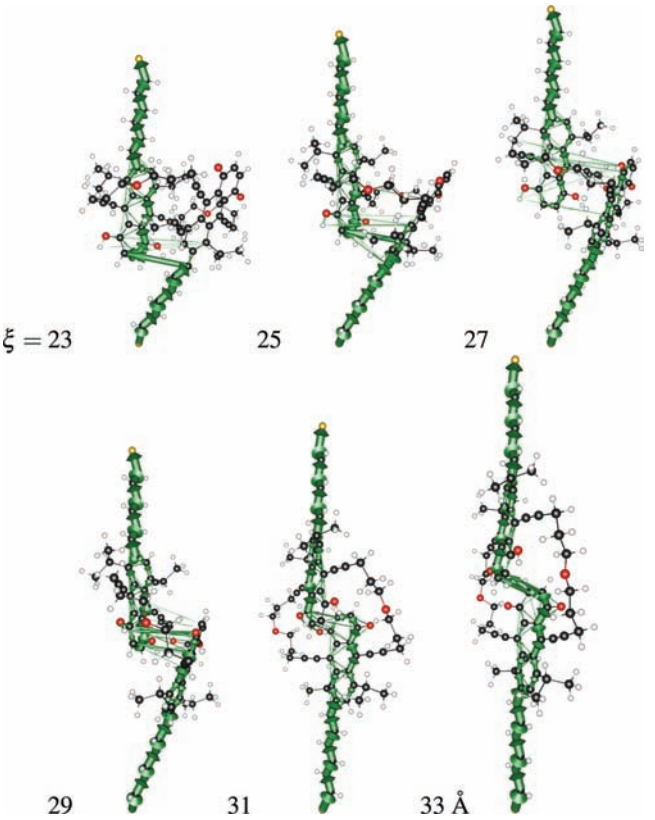

Figure 4. Average local transmission as a function of molecular elongation. The plots depict the local transmission averaged over 4000 geometries for several values of ξ. Arrows (solid green) represent the local transmission elements.The radius of each arrow is determined by the magnitude of the transmission element it represents. Plots are normalized so that the S−C components (which are generally very close to the total transmission) are the same in every plot. The total average transmission in each case is shown in Figure 3.

The decomposition assumes an atom-centered localized basis set to obtain a current between pairs of atoms in the zero temperature limit of the Landauer formalism. While only the total current across a given surface can be experimentally observed, in the zero-bias limit the T_{AB} values offer a measure of how much current passes through atoms A and B and are useful in interpreting transport results and in molecular design.[30,55] Figure 4 shows the thermal average of the local transmission elements at the Fermi energy $\langle T_{AB}(E_F)\rangle$ for different molecular end-to-end distances. In the plots, the T_{AB} values are plotted as arrows with a radius determined by the relative magnitude of the transmission element it represents with respect to the total average transmission at that particular extension. Since the local current analysis is based on a coherent tunneling mechanism, the arrows representing the local transmission elements should not be interpreted as an electron hopping through the molecule. Rather, the arrows show graphically the transmission resulting from the sum over all pathways through the molecule that are responsible for mediating the tunneling; effectively controlling the nature of the tunneling barrier. Further note that even when the local transmission elements are plotted in the figure on specific (minimum energy) geometries, they represent the average transport characteristics of the ensemble of geometries that are consistent with each molecular elongation.

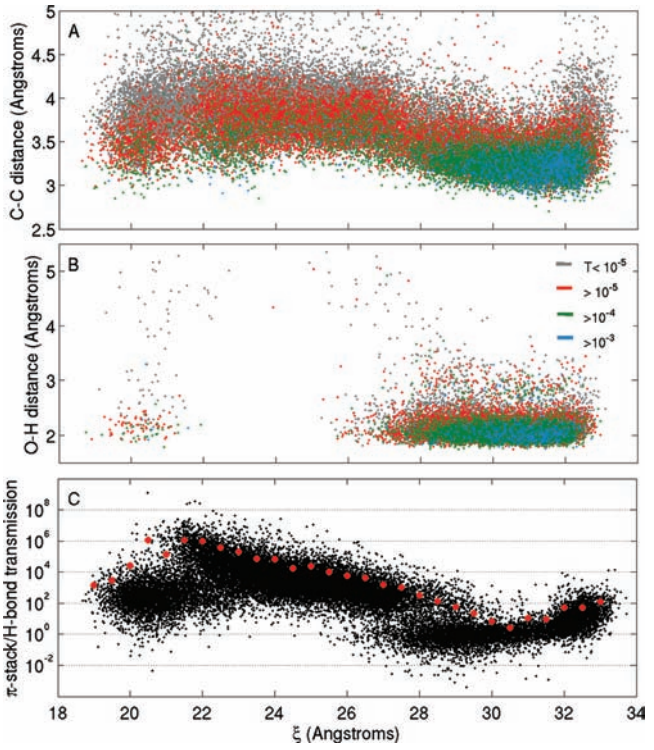

Figure 5. Average distance between pairs of carbon atoms (A) and hydrogen-bonded atoms (B) with local transmission elements $T_{AB}(E_F) > 20\%$ of the total transmission between the complementary rings. The color of the dots indicates the magnitude of the total transmission for each particular configuration. The relative importance of the transmission across the π-stack with respect to the transmission through hydrogen bonds can be seen from the ratio of the two shown in (C) (black dots, raw data; red dots, average behavior in 0.5 Å bins).

For ξ = 23 Å, the cyclophane is compressed and electronic transport across the molecule is dominated by the interactions between the dihydroxyanthracene and the alkene chain connected to the anthraquinone. As the elongation proceeds (ξ = 25 and 27 Å) the plots indicate that transport is dominated by interactions between the two complementary rings. The transmission is not very efficient since the *t*-Bu groups prevent stacked alignment between the rings. For ξ = 29 and 31 Å, the *t*-Bu groups no longer prevent stacking and the H-bonds promote π-stacking. The $\langle T_{AB}(E_F)\rangle$ values show that the transport goes through the terminal rings of both aromatic units. At these extensions both π-stacks and H-bonds contribute as paths to the total transmission. For longer extensions (ξ = 33 Å), the hydrogen bonds are disrupted and transport is only possible between terminal carbon atoms in each of the complementary rings, leading to a natural decrease in the total transmission with elongation.

It is also possible to qualitatively characterize the relative contributions of different modes of transport across the complementary rings. Figure 5 shows the average distance between pairs of either carbon atoms (A) or hydrogen-bonded atoms (B) that are dominant in mediating the transport across the stacks. A pair is deemed dominant if $T_{AB}(E_F) > 20\%$ of the total transmission between the complementary rings. As shown in Figure 5A, the average distance between carbon atoms responsible for mediating the transport decreases with molecular elongation. It is this counterintuitive conformational change that

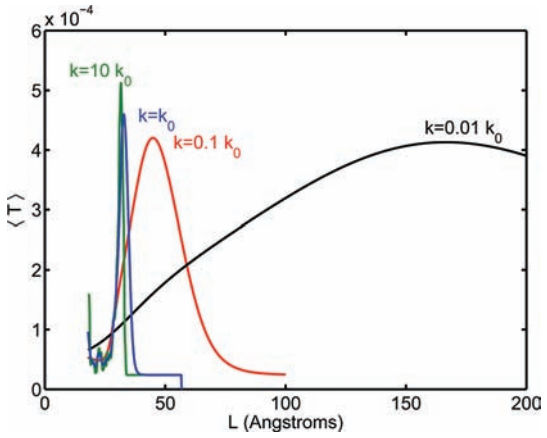

Figure 6. Average transmission during pulling using cantilevers of varying stiffness *k*. Here k_0 = 1.1 N/m is the stiffness employed in the simulations.

itself underlies the inverted trend for transport as a function of length. In turn, dominant pairs of hydrogen-bonded atoms only appear when the system π-stacks at longer values of ξ, and for them, the distance between the atoms in the pair is approximately constant. These two metrics together indicate that the total transmission peaks when the complementary rings are π-stacked with the hydrogen bonds stabilizing the stack and contributing to the transport.

Previously,[30] we had observed that hydrogen bonds can play a significant role in carrying current through stacked systems, raising the question of how much of the increased transmission is due to hydrogen-bond-mediated transport. Figure 5C shows the ratio of the sum of the local transmission elements between all pairs of carbon atoms across the stack over the sum of local transmission elements between all hydrogen-bonded pairs. The black dots correspond to the raw data, while the red circles indicate the average behavior. Around the transmission maximum at $\xi \approx 31.5$ Å the carbon−carbon interactions contribute on average 10 times more to the transport than the hydrogen-bonded interactions. Away from the region of maximum transmission (30 Å < ξ < 32 Å) the carbon−carbon interactions completely dominate the transport. This picture illustrates the dual role that the hydrogen bonds can play in this system, stabilizing the π-stack (thereby maximizing the transport mediated by the carbon−carbon interactions) while simultaneously introducing further electronic coupling across the stack that also enhances transport.

While it is possible to further analyze the local transmission for particular conformations, it is difficult to make general conclusions that go beyond those outlined above. The local transmission fluctuates with the total transmission and varies over orders of magnitude, both at a given ξ and with extension. As with the total transmission, it is perilous to make conclusions about the behavior of the ensemble from the behavior of isolated conformations and it is prudent to only study the local transmission either when it is averaged over conformations or when all conformations are considered.

The *T* vs *L* curves recorded during pulling depend on the cantilever stiffness employed. This is because the fluctuations in the end-to-end distance increase with decreasing cantilever stiffness (in the simplest harmonic model $d\xi \approx (k_B T/k)^{1/2}$). To quantify such dependence, recall[34] that the pulling process

can be viewed as thermal motion along an effective one-dimensional potential $U_L(\xi) = \phi(\xi) + V_L(\xi)$ determined by the PMF $\phi(\xi)$ and the cantilever potential $V_L(\xi) = k(\xi - L)^2/2$. Using the reconstructed PMF (Figure 2) and the average behavior of the transmission as a function of ξ $[T(\xi)]$, one can then calculate $T-L$ curves when pulling with cantilevers of arbitrary stiffness as $\langle T(L)\rangle = \int d\xi\, T(\xi) \exp[-U_L(\xi)/k_BT / \int d\xi \exp[-U_L(\xi)/k_BT]$. Figure 6 shows the transport−extension behavior of the cyclophane when pulling using cantilevers of varying stiffness. For stiff k (green line), $L \approx \xi$ and the average transmission-extension profile shown in Figure 3 is recovered. As k is made softer, a longer L is required to pull the cyclophane to its highly conducting state, and in addition, the maximum $\langle T\rangle$ observed decreases due to the inherent averaging that arises when ξ fluctuates. We observe that the basic counterintuitive behavior in which the transmission increases with applied force is robust to changes in the cantilever stiffness over at least 4 orders of magnitude.

FINAL REMARKS

The integration of single-molecule pulling with molecular electronics makes it possible to access, in a controlled fashion and with subangstrom resolution, molecular conformations that cannot be probed in an unbiased setting. This control over the molecular conformation effectively adds a new dimension to molecular electronics and opens the way to design a whole series of mechanically activated molecular devices. In this paper we have introduced a molecular system with an exotic transport−extension behavior in which the tunneling currents increase with molecular elongation. This inverted trend contrasts with the usual decay of tunneling currents with increased molecular length, and it is achieved by using a molecular architecture with transport-determining electronic couplings that are enhanced under applied force. Interestingly, a similar trend has recently been proposed[57] to be observable in DNA strands where large applied forces can induce a structure in which the nucleobases from the opposite DNA strands interdigitate, forming a continuous aromatic stack[58] with enhanced charge transport characteristics.

The simulations reveal how correlated force−transport properties can be highly discriminating with regard to the behavior of molecules in junctions. The force measurements signal major conformational transitions that occur during pulling, while conductance measurements are exponentially sensitive to those changes in the conformation that determine electronic through-molecule transport. In the case of the molecule considered, regions of mechanical instability revealed conformational transitions that are not evident in the average conductance, while the transport properties signal optimal stacking between the complementary aromatic rings in a region where the force−extension isotherm is relatively featureless.

In addition, the results presented highlight the importance of proper statistical sampling in molecular electronics computations of pulled and unpulled systems. Thermal motion of the molecule can induce fluctuations in the transport properties over several orders of magnitude, an observation that is consistent with studies of the role of fluctuations in electron transfer in biological systems.[52−54] Average transport can be dominated by a relatively small subset of conformations with a high transmission[28,30] and not necessarily by the minimum energy conformations.

ASSOCIATED CONTENT

Supporting Information. Additional MM3 parameters required to describe the molecule in Scheme 1. This material is available free of charge via the Internet at http://pubs.acs.org/.

AUTHOR INFORMATION

Corresponding Author
ifranco@chem.northwestern.edu; ratner@chem.northwestern.edu

ACKNOWLEDGMENT

We thank Christopher B. George for useful discussions. This work was supported by the Nonequilibrium Energy Research Center (NERC), which is an Energy Frontier Research Center funded by the U.S. Department of Energy, Office of Science, Office of Basic Energy Sciences, under Award Number DE-SC0000989. G.C. Solomon gratefully acknowledges funding from The Danish Council for Independent Research Natural Sciences.

REFERENCES

(1) Datta, S. *Quantum Transport: Atom to Transistor*; Cambridge University Press: New York, 2005.
(2) Joachim, C.; Gimzewski, J. K.; Aviram, A. *Nature* **2000**, *408*, 541–548.
(3) Nitzan, A. *Annu. Rev. Phys. Chem.* **2001**, *52*, 681–750.
(4) Nitzan, A.; Ratner, M. A. *Science* **2003**, *300*, 1384–1389.
(5) Joachim, C.; Ratner, M. A. *Proc. Natl. Acad. Sci. U.S.A.* **2005**, *102*, 8801–8808.
(6) Galperin, M.; Ratner, M. A.; Nitzan, A.; Troisi, A. *Science* **2008**, *319*, 1056–1060.
(7) Chen, F.; Tao, N. J. *Acc. Chem. Res.* **2009**, *42*, 429–438.
(8) Davis, W. B.; Svec, W. A.; Ratner, M. A.; Wasielewski, M. R. *Nature* **1998**, *396*, 60–63.
(9) Giese, B.; Amaudrut, J.; Kohler, A.-K.; Spormann, M.; Wessely, S. *Nature* **2001**, *412*, 318–320.
(10) Ho Choi, S.; Kim, B.; Frisbie, C. D. *Science* **2008**, *320*, 1482–1486.
(11) Choi, S. H.; Risko, C.; Delgado, M. C. R.; Kim, B.; Brédas, J.-L.; Frisbie, C. D. *J. Am. Chem. Soc.* **2010**, *132*, 4358–4368.
(12) Hines, T.; Diez-Perez, I.; Hihath, J.; Liu, H.; Wang, Z.-S.; Zhao, J.; Zhou, G.; Müllen, K.; Tao, N. *J. Am. Chem. Soc.* **2010**, *132*, 11658–11664.
(13) Schneebeli, S. T.; Kamenetska, M.; Cheng, Z.; Skouta, R.; Friesner, R. A.; Venkataraman, L.; Breslow, R. *J. Am. Chem. Soc.* **2011**, *133*, 2136–2139.
(14) Segal, D.; Nitzan, A.; Davis, W. B.; Wasielewski, M. R.; Ratner, M. A. *J. Phys. Chem. B* **2000**, *104*, 3817–3829.
(15) Berlin, Y. A.; Burin, A. L.; Ratner, M. A. *Chem. Phys.* **2002**, *275*, 61–74.
(16) Grozema, F. C.; Tonzani, S.; Berlin, Y. A.; Schatz, G. C.; Siebbeles, L. D. A.; Ratner, M. A. *J. Am. Chem. Soc.* **2008**, *130*, 5157–5166.
(17) Magoga, M.; Joachim, C. *Phys. Rev. B* **1998**, *57*, 1820–1823.
(18) Paul, A.; Watson, R. M.; Wierzbinski, E.; Davis, K. L.; Sha, A.; Achim, C.; Waldeck, D. H. *J. Phys. Chem. B* **2010**, *114*, 14140–14148.
(19) Lu, Q.; Liu, K.; Zhang, H.; Du, Z.; Wang, X.; Wang, F. *ACS Nano* **2009**, *3*, 3861–3868.
(20) Johnson, M. D.; Miller, J. R.; Green, N. S.; Closs, G. L. *J. Phys. Chem.* **1989**, *93*, 1173–1176.
(21) Xu, B.; Tao, N. J. *Science* **2003**, *301*, 1221–1223.
(22) Park, Y. S.; Whalley, A. C.; Kamenetska, M.; Steigerwald, M. L.; Hybertsen, M. S.; Nuckolls, C.; Venkataraman, L. *J. Am. Chem. Soc.* **2007**, *129*, 15768–15769.

(23) Chu, C.; Na, J.-S.; Parsons, G. N. *J. Am. Chem. Soc.* **2007**, *129*, 2287–2296.
(24) Lafferentz, L.; Ample, F.; Yu, H.; Hecht, S.; Joachim, C.; Grill, L. *Science* **2009**, *323*, 1193–1197.
(25) Quek, S. Y.; Kamenetska, M.; Steigerwald, M. L.; Choi, H. J.; Louie, S. G.; Hybertsen, M. S.; Neaton, J. B.; Venkataraman, L. *Nat. Nanotechnol.* **2009**, *4*, 230–234.
(26) Frei, M.; Aradhya, S. V.; Koentopp, M.; Hybertsen, M. S.; Venkataraman, L. *Nano Lett.* **2011**, *11*, 1518–1523.
(27) Chang, S.; He, J.; Kibel, A.; Lee, M.; Sankey, O.; Zhang, P.; Lindsay, S. *Nat. Nanotechnol.* **2009**, *4*, 297–301.
(28) Lin, J.; Beratan, D. N. *J. Phys. Chem. A* **2004**, *108*, 5655–5661.
(29) Paulsson, M.; Krag, C.; Frederiksen, T.; Brandbyge, M. *Nano Lett.* **2009**, *9*, 117–121.
(30) Franco, I.; George, C. B.; Solomon, G. C.; Schatz, G. C.; Ratner, M. A. *J. Am. Chem. Soc.* **2011**, *133*, 2242–2249.
(31) Diez-Perez, I.; Hihath, J.; Hines, T.; Wang, Z.-S.; Zhou, G.; Mullen, K.; Tao, N. *Nat. Nano* **2011**, *6*, 226–231.
(32) Parks, J. J.; Champagne, A. R.; Costi, T. A.; Shum, W. W.; Pasupathy, A. N.; Neuscamman, E.; Flores-Torres, S.; Cornaglia, P. S.; Aligia, A. A.; Balseiro, C. A.; Chan, G. K.-L.; Abruña, H. D.; Ralph, D. C. *Science* **2010**, *328*, 1370–1373.
(33) Li, X.; He, J.; Hihath, J.; Xu, B.; Lindsay, S. M.; Tao, N. *J. Am. Chem. Soc.* **2006**, *128*, 2135–2141.
(34) Franco, I.; Schatz, G. C.; Ratner, M. A. *J. Chem. Phys.* **2009**, *131*, 124902.
(35) Allinger, N. L.; Yuh, Y. H.; Lii, J. H. *J. Am. Chem. Soc.* **1989**, *111*, 8551–8566.
(36) Lii, J. H.; Allinger, N. L. *J. Am. Chem. Soc.* **1989**, *111*, 8566–8575.
(37) Lii, J. H.; Allinger, N. L. *J. Am. Chem. Soc.* **1989**, *111*, 8576–8582.
(38) Ponder, J. *TINKER: Software Tools for Molecular Design 4.2*; Washington University School of Medicine: Saint Louis, MO, 2004.
(39) Franco, I.; Ratner, M. A.; Schatz, G. C. *J. Phys. Chem. B* **2011**, *115*, 2477–2484.
(40) Elstner, M.; Porezag, D.; Jugnickel, G.; Elsner, J.; Haugk, M.; Frauenheim, T.; Suhai, S.; Seifert, G. *Phys. Rev. B* **1998**, *58*, 7260–7268.
(41) Frauenheim, T.; Seifert, G.; Elstner, M.; Hagnal, Z.; Jungnickel, G.; Porezag, D.; Suhai, S.; Scholz, R. *Phys. Status Solidi B* **2000**, *217*, 41–62.
(42) Frauenheim, T.; Seifert, G.; Elstner, M.; Niehaus, T.; Koehler, C.; Amkreutz, M.; Sternberg, M.; Hajnal, Z.; Di Carlo, A.; Suhai, S. *J. Phys.: Condens. Matter* **2002**, *14*, 3015–3047.
(43) Porezag, D.; Frauenheim, T.; Kohler, T.; Seifert, G.; Kaschner, R. *Phys. Rev. B* **1995**, *51*, 12947–12957.
(44) Pecchia, A.; Di Carlo, A. *Rep. Prog. Phys.* **2004**, *67*, 1497–1561.
(45) Bilic, A.; Reimers, J. R.; Hush, N. S. *J. Chem. Phys.* **2005**, *122*, 094708–094715.
(46) Andrews, D. Q.; Van Duyne, R. P.; Ratner, M. A. *Nano Lett.* **2008**, *8*, 1120–1126.
(47) Ferrenberg, A. M.; Swendsen, R. H. *Phys. Rev. Lett.* **1989**, *63*, 1195–1198.
(48) Kumar, S.; Bouzida, D.; Swendsen, R. H.; Kollman, P. A.; Rosenberg, J. M. *J. Comput. Chem.* **1992**, *13*, 1011–1021.
(49) Kang, Y. K.; Rubtsov, I. V.; Iovine, P. M.; Chen, J.; Therien, M. J. *J. Am. Chem. Soc.* **2002**, *124*, 8275–8279.
(50) Zheng, J.; Kang, Y. K.; Therien, M. J.; Beratan, D. N. *J. Am. Chem. Soc.* **2005**, *127*, 11303–11310.
(51) Kang, Y. K.; Iovine, P. M.; Therien, M. J. *Coord. Chem. Rev.* **2011**, *255*, 804–824.
(52) Skourtis, S. S.; Waldeck, D. H.; Beratan, D. N. *Annu. Rev. Phys. Chem.* **2010**, *61*, 461–485.
(53) Balabin, I. A.; Beratan, D. N.; Skourtis, S. S. *Phys. Rev. Lett.* **2008**, *101*, 158102.
(54) Hatcher, E.; Balaeff, A.; Keinan, S.; Venkatramani, R.; Beratan, D. N. *J. Am. Chem. Soc.* **2008**, *130*, 11752–11761.
(55) Solomon, G. C.; Herrmann, C.; Hansen, T.; Mujica, V.; Ratner, M. A. *Nat. Chem.* **2010**, *2*, 223–228.
(56) Todorov, T. N. *J. Phys.: Condens. Matter* **2002**, *14*, 3049–3084.
(57) Balaeff, A.; Craig, S. L.; Beratan, D. N. *J. Phys. Chem. A* **2011**, *115*, 9377–9391.
(58) Lohikoski, R.; Timonen, J.; Laaksonen, A. *Chem. Phys. Lett.* **2005**, *407*, 23–29.